Nonlinear Dyn (2016) 85:2233–2245
DOI 10.1007/s11071-016-2825-y

ORIGINAL PAPER

Nonlinear behaviors as well as the mechanism in a piecewise-linear dynamical system with two time scales

Qinsheng Bi · Xiaoke Chen · Juergen Kurths · Zhengdi Zhang

Received: 11 August 2015 / Accepted: 28 April 2016 / Published online: 23 May 2016

Abstract The main purpose of the work was to explore the bursting oscillations as well as the mechanism in a periodically excited piecewise-linear system with an order gap between the exciting frequency and the natural frequency. Based on the typical Chua's circuit, a periodically excited model is established, in which the nonlinear characteristics of the resistor are expressed in terms of a continuous function with multiple piecewise-linear segments. By analyzing the nominal equilibrium orbits of the linear subsystems in different regions divided by the break points, critical conditions corresponding to regular and non-smooth bifurcations are derived. Two typical cases in which the trajectories pass across different numbers of non-smooth boundaries are investigated, resulting in different forms of bursting oscillations. It is pointed that not only the properties of the nominal equilibrium orbits in different regions but also the non-smooth boundaries may influence the bursting attractors. Furthermore, unlike the connections between quiescent states (**QS**s) and spiking states (**SP**s) via regular bifurcations in smooth vector fields, for the bursting oscillations in piecewise-linear systems, the transitions between **QS**s and **SP**s may be caused by non-smooth bifurcations or the abrupt alternations between two different subsystems on both sides of the non-smooth boundaries.

Keywords Bursting oscillation · Non-smooth bifurcation · Piecewise-linear · Bifurcation mechanism

Q. Bi (✉)· X. Chen · Z. Zhang
Faculty of Science, Jiangsu University, Zhenjiang 212013, People's Republic of China
e-mail: qbi@ujs.edu.cn

J. Kurths
Potsdam Institute for Climate Impact Research, Telegrafenberg A31, 14473 Potsdam, Germany

1 Introduction

Many dynamical systems in natural and engineering problems involve two timescales [1,2], which often behave in periodic states characterized by a combination of relatively large-amplitude and nearly harmonic small-amplitude oscillations, conventionally denoted by N^K with N and K corresponding to large- and small-amplitude oscillations, respectively [3,4]. Generally, the system is in a quiescent state (**QS**) stage when all the variables are at rest or exhibit small-amplitude oscillations [5]. The coupling of two timescales may lead the systems to spiking state (**SP**), in which the variables may behave in large-amplitude oscillations [6,7]. Bursting phenomena can be observed when the variables alternate between **QS** and **SP**. Two important bifurcations associated with the bursting exist: bifurcation of a quiescent state to repetitive spiking oscillations and bifurcation of a spiking state to a quiescent state [8,9].

Since the bursting oscillations in a famous slow–fast Hodgkin–Huxley model were presented, which can approach nero activities [10,11], a lot of reports related to the dynamics with two timescales have been

published [12,13], in which several types of bursting oscillations such as the fold/fold [14] and fold/Hopf [15] bursters have been obtained. However, most of the results were focused on autonomous systems with different scales in time domain, in which the vector fields can be divided into two subsystems, i.e., a slow subsystem and a fast subsystem [16]. Based on the so-called slow–fast analysis [17], bursting oscillations may be divided into different types according to the bifurcation forms between **QS**s and **SP**s. However, for non-autonomous systems, such as periodic excited systems, when an order gap exists between the frequency of periodic excitation and natural frequency, implying two scales in frequency domain exist, no obvious slow and fast subsystem exists, while the effect of two timescales can also be observed [18], based on the fact that the trajectories of systems are related to both the two frequencies [19], behaving in relaxation oscillations [20]. Since no obvious slow and fast subsystem exists, the method of slow–fast analysis cannot be directly employed to approach the mechanism of the bursting. How to explore the characteristics of multi-mode oscillations in non-autonomous system still remains an open problem.

For a typical periodically excited dynamical system, when the exciting term changes on a much smaller timescale comparing with the change in state variables, the whole exciting term can be regarded as a slow-varying parameter, leading to a so-called generalized autonomous, and a transformed phase portrait can be employed to explore the influence of the exciting term on the evolution of the dynamical behavior [21].

Furthermore, when piecewise-linear functions with multiple segments involve the vector fields, multiple non-smooth boundaries corresponding to the cross sections determined by the break points exist, which divide the phase space into several regions associated with different subsystems with different dynamical behaviors [22,23]. Not only the attractors as well as the bifurcations in the subsystems, but also the non-smooth bifurcations for the trajectories passing across the break points may influence the structures of the bursting oscillations [24,25]. How to explore the bifurcation mechanism of the bursting oscillations for such kind of dynamical systems, especially when the trajectories pass across different numbers of non-smooth boundaries, still needs to be explored.

Here, we try to investigate these problems upon a relative simple model by introducing a periodically changed electric current source to excite the typical Chua's oscillator [26] in which the characteristics of the resistor can be described by a continuous piecewise-linear function with multiple segments. By taking suitable parameter values so that an order gap exists between the exciting frequency and the natural frequency, the evolution of the dynamics of the system is investigated and different types of bursting oscillations as well as bifurcation mechanism for the trajectory passing across different numbers of break points will be presented.

2 Mathematical model

By introducing a periodically changed electrical current source in a typical Chua's circuit with piecewise-linear characteristic nonlinear resistor [26], shown in Fig. 1, the related mathematical model can be expressed as

$$\begin{aligned}
\frac{\mathrm{d}V_1}{\mathrm{d}t} &= \tfrac{1}{C_1}[G_1(V_2 - V_1) - g(V_1) + I_G \sin(\omega t)],\\
\frac{\mathrm{d}V_2}{\mathrm{d}t} &= \tfrac{1}{C_2}[G_1(V_1 - V_2) + i_L],\\
\frac{\mathrm{d}i_L}{\mathrm{d}t} &= -\tfrac{1}{L_1}V_2,
\end{aligned} \tag{1}$$

where i_L is the current value passing across two inductors with values L_1, V_1 and V_2 measure the magnitudes of voltage of the two capacitors with values C_1 and C_2, respectively, while $G_1 = 1/R_1$ and R_1 is the resistance value. I_G and ω correspond to the amplitude and the frequency of the current through the electric source G with $I_S = I_G \sin(\omega t)$. $g(V_1) = \frac{1}{R_1}[\delta V_1 + F(V_1)]$ describes the relationship between the current and the voltage passing across the nonlinear resistor N_R. $F(V_i)$ is a piecewise-linear function with multiple segments in symmetry, expressed in the form

$$F(V_1) = \begin{cases} S_i(V_1 - E_i), & V_1 \in [P_i, P_{i+1}],\ (i = 1, 2, \ldots),\\ S_0(V_1 - E_0), & V_1 \in [-P_1, P_1],\\ S_i(V_1 + E_i), & V_1 \in [-P_{i+1}, -P_i],\ (i = 1, 2, \ldots), \end{cases} \tag{2}$$

where $E_0 = 0$, while $E_i > 0$ and $P_i > 0$, satisfying $E_i < E_{i+1}$ and $P_i < P_{i+1}$, $(i = 1, 2, \ldots)$, in which P_i denotes the voltage values at the break points.

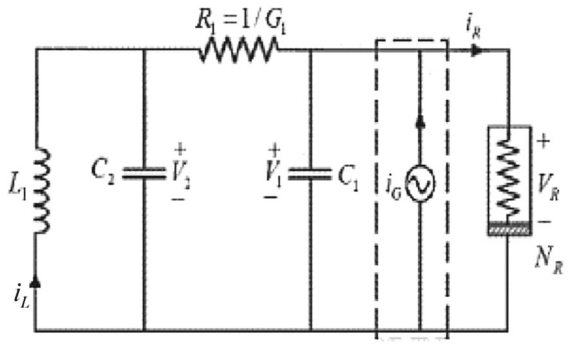

Fig. 1 Chua's circuit with periodic excitation

By introducing the transformations $x = \frac{V_1}{E_1}$, $y = \frac{V_2}{E_1}$, $z = \frac{i_L}{E_1 R_1}$ and $\tau = \frac{t}{R_1 C_2}$, (1) can be written in a non-dimensional form as

$$\begin{aligned} \frac{\mathrm{d}x}{\mathrm{d}\tau} &= -\alpha(1+\delta)x + \alpha y - \alpha f(x) + A\sin(\Omega\tau), \\ \frac{\mathrm{d}y}{\mathrm{d}\tau} &= x - y + z, \\ \frac{\mathrm{d}z}{\mathrm{d}\tau} &= -\beta y \end{aligned} \tag{3}$$

where $\alpha = \frac{C_2}{C_1}$, $\beta = \frac{R_1^2 C_2}{L_1}$, $A = \frac{I_G R_1 E_1 C_2}{C_1}$, $\Omega = \omega R_1 C_2$ and $f(x)$ can be written as

$$f(x) = \begin{cases} m_i(x - k_i), & x \in [Q_i, Q_{i+1}],\ (i = 1, 2, \ldots), \\ m_0(x - k_0), & x \in [-Q_1, Q_1], \\ m_i(x + k_i), & x \in [-Q_{i+1}, -Q_i],\ (i = 1, 2, \ldots), \end{cases} \tag{4}$$

with $m_0 = \frac{S_0}{E_1}$, $k_0 = 0$, $m_i = \frac{S_i}{E_1}$,$k_i = \frac{E_i}{E_1}$, $Q_i = \frac{P_i}{E_1}$, $(i = 1, 2, \ldots)$. System (3) with no external excitation ($A = 0$) may evolve from a stable fixed point to a periodic orbit and to a double scroll, i.e., the strange attractor of Chua's circuit, with the variation in parameters for the two break points of the piecewise-linear resistor [27]. Furthermore, a n-scroll attractor family was obtained as a result of generalization of Chua's circuit with additional break points in the nonlinear characteristic of Chua's diode [28]. Due to the generalization of the nonlinear characteristics, it has been shown that increasing the number of scrolls in all state variable directions is also possible [29].

The external excitation may also cause the oscillator to evolve from a periodic orbit to n-scroll attractors. However, when an order gap exists between Ω and the natural frequency of the autonomous oscillator, effects of two timescales may appear. Here, we fix the parameter $\Omega = 0.01$ and other parameters at $O(1.0)$. Obviously, the state variables x, y, z may oscillate mainly according to the natural frequency, i.e., $O(\mathrm{d}x/\mathrm{d}\tau, \mathrm{d}y/\mathrm{d}\tau, \mathrm{d}z/\mathrm{d}\tau) \approx O(1.0) \equiv T_1$, while the exciting term w oscillates periodically according to another much smaller scale, i.e., $O(\mathrm{d}w/\mathrm{d}\tau) \approx O(0.01) \equiv T_2$, leading to a coupling between the two scales T_1 and T_2, which may cause bursting oscillations in the system.

3 Bifurcation analysis

Since there exists only one nonlinear term included in the piecewise-linear function in the oscillator, between each two neighboring break points, the vector field is linear, though non-smooth behaviors may appear at the break points. Therefore, one may obtain a set of corresponding linear subsystems according to the situation of the piecewise-linear function. The steady states of these linear subsystems in periodic movements may be employed to understand the behaviors of the whole system (3), which here are called nominal equilibrium orbits (**NEO**).

3.1 Nominal equilibrium orbits (**NEO**)

For the linear subsystems with the periodic excitation $A\sin(\Omega\tau)$, the nominal equilibrium orbits (**NEO**) can be expressed in the form

$$\begin{cases} x = X_0 + A_1\sin(\Omega\tau + \theta_1), \\ y = Y_0 + A_2\sin(\Omega\tau + \theta_2), \\ z = Z_0 + A_3\sin(\Omega\tau + \theta_3), \end{cases} \tag{5}$$

where $X_0, Y_0, Z_0, A_i, \theta_i,\ (i = 1, 2, 3)$ are constants to be determined by balancing the same terms of each corresponding linear equations. For example, the constants related to $\mathbf{NEO}_i$ in the form (5) for the segment with $f(x) = m_i(x - k_i)$ of the piecewise-linear function $f(x)$ can be expressed as

$$\begin{aligned} X_0 &= \tfrac{m_i k_i}{\Pi_1}, \quad Y_0 = 0, \quad Z_0 = -\tfrac{m_i k_i}{\Pi_1}, \\ A_1 &= \frac{A\sqrt{\Pi_1}}{\sqrt{\alpha^2\Pi_2\Pi_1^2 - 2\alpha^2\Omega^2\Pi_1 + \Omega^2(\Pi_2 + \alpha^2 - 2\alpha\beta + 2\alpha\Omega^2)}}, \\ A_2 &= \frac{A\Omega}{\sqrt{\alpha^2\Pi_2\Pi_1^2 - 2\alpha^2\Omega^2\Pi_1 + \Omega^2(\Pi_2 + \alpha^2 - 2\alpha\beta + 2\alpha\Omega^2)}}, \\ A_3 &= \frac{A\beta}{\sqrt{\alpha^2\Pi_2\Pi_1^2 - 2\alpha^2\Omega^2\Pi_1 + \Omega^2(\Pi_2 + \alpha^2 - 2\alpha\beta + 2\alpha\Omega^2)}}, \\ \theta_1 &= \arctan\left[\frac{\Omega(\alpha\beta - \alpha\Omega^2 - \Pi_2)}{\alpha\Pi_1\Pi_2 - \Omega^2}\right], \\ \theta_2 &= \arctan\left[\frac{\alpha\Pi_1(\beta - \Omega^2) - \Omega^2}{\Omega(\beta - \Omega^2 - \alpha - \alpha\Pi_1)}\right], \\ \theta_3 &= \tfrac{\pi}{2} - \theta_2, \end{aligned} \tag{6}$$

where $\Pi_1 = 1 + \delta + m_i, \Pi_2 = \Omega^2 + (\beta - \Omega^2)^2$. The associated characteristic equation can be written as

$$\lambda^3 + (1 + \alpha\Pi_1)\lambda^2 + (\beta - \alpha - \alpha\Pi_1)\lambda + \alpha\beta\Pi_1 = 0, \tag{7}$$

which yields the nominal stability condition, given as

$$\begin{cases} 1 + \alpha\Pi_1 > 0, \quad \alpha\beta\Pi_1 > 0, \\ \alpha\beta\Pi_1 - (1 + \alpha\Pi_1)(\beta - \alpha + \alpha\Pi_1) > 0, \end{cases} \tag{8}$$

implying that when the conditions in (6) are satisfied, the trajectory may settle down to the **NEO**$_i$ once $Q_i < x < Q_{i+1}$.

3.2 Bifurcations

There may exist two types of bifurcations related to **NEO**s: the regular bifurcations and the non-smooth bifurcations. The regular bifurcations may occur when at least the real part of one eigenvalue related to **NEO**s becomes zero, which may cause the change in the properties of **NEO**s. Two critical conditions related to codimension-1 bifurcations of **NEO**s can be obtained. One can be expressed as

$$\textbf{FB:} \quad 1 + \alpha\Pi_1 = 0, \tag{9}$$

with $\alpha\beta\Pi_1 > 0$, $\alpha\beta\Pi_1 - (1+\alpha\Pi_1)(\beta-\alpha+\alpha\Pi_1) > 0$, at which a zero eigenvalue can be obtained, implying a fold bifurcation of the limit cycle may occur, while the other can be written as

$$\textbf{HB:} \quad \alpha\beta\Pi_1 - (1 + \alpha\Pi_1)(\beta - \alpha + \alpha\Pi_1) = 0, \tag{10}$$

with $1 + \alpha\Pi_1 > 0$, $\alpha\beta\Pi_1 > 0$, at which a pair of pure imaginary eigenvalues exists, leading to Hopf bifurcation of the limit cycle.

When the trajectory passes across the break points, non-smooth bifurcations may take place, which can be explored by the generalized differential of Clarke [30]. Assuming J_i and J_{i+1} denote the two Jacobian matrices of a equilibrium state on both sides of a non-smooth boundary, respectively, then the generalized Jacobian matrix at the break point can be expressed as $J_q = qJ_i + (1 - q)J_{i+1}$, where q is an auxiliary parameter with $q \in [0, 1]$. When q varies from 0 to 1, J_q may change from J_{i+1} to J_i, implying the parameter q causes the smooth transition of Jacobian matrix from one side to the other side of the non-smooth boundary.

When at least one of the eigenvalues of J_q passes across axes for q varying from 0 to 1, a non-smooth bifurcation may take place. Note that the Jacobian matrix related to **NEO**$_i$ can be written in the form

$$J_i = \begin{pmatrix} -\alpha(1 + \delta + m_i) & \alpha & 0 \\ 1 & -1 & 1 \\ 0 & -\beta & 0 \end{pmatrix}. \tag{11}$$

By introducing the auxiliary parameter q, the characteristic equation of the generalized Jacobian matrix related to the break point Q_{i+1} can be expressed as $J_q = qJ_i + (1 - q)J_{i+1}$ $q \in [0, 1]$, which can be further written in the form

$$\lambda^3 + h_1\lambda^2 + h_2\lambda + h3 = 0, \tag{12}$$

where

$$\begin{aligned} h_1 &= 1 + \alpha + \delta + \alpha(q\, m_i + m_{i+1} - q\, m_{i+1}), \\ h_2 &= \alpha\delta + \beta + \alpha(q\, m_i + m_{i+1} - q\, m_{i+1}), \\ h_3 &= \alpha\beta(1 + \delta + q\, m_i + m_{i+1} - q\, m_{i+1}). \end{aligned} \tag{13}$$

Similarly, with the variation in q from 0 to 1, the eigenvalues of the generalized Jacobian may pass across the axes, leading to two types of non-smooth bifurcations with codimension-1. For the conditions

$$\textbf{NSHB:} \quad h_3 = 0, \ (h_1 > 0, \ \ h_1 h_2 - h_3 > 0), \tag{14}$$

a zero eigenvalue appears, implying a non-smooth fold bifurcation of **NEO**$_i$ may be observed at the break point Q_{i+1}, while a non-smooth Hopf bifurcation of **NEO**$_i$ may take place when

$$\textbf{NSHB:} \quad h_1 h_2 - h_3 = 0, \ (h_1 > 0, \ \ h_3 > 0). \tag{15}$$

at which a pair of pure imaginary eigenvalues can be obtained.

Remarks:

- The bifurcations at the break points are different from the same types of bifurcations in smooth vector fields, though the influence of the bifurcations on the trajectories of the dynamical system may be similar.

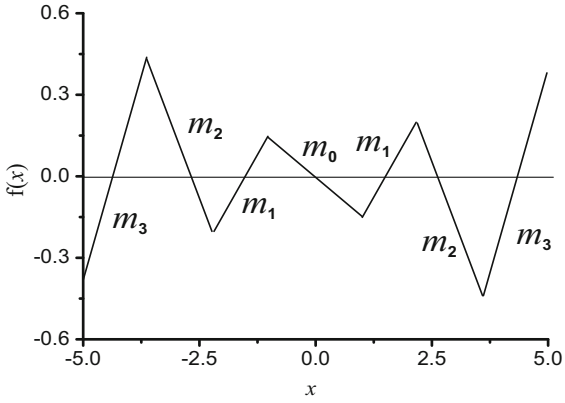

Fig. 2 Characteristics of piecewise-linear function

- Theoretically, there may also exist other types of non-smooth bifurcations such as non-smooth Bogdanov–Takens bifurcation of cycle for $h_2 = 0, h_3 = 0 (h_1 > 0)$.
- Multiple crossing bifurcation with high codimension may be observed when the conditions for two types of bifurcations are satisfied for the auxiliary parameter q varying from 0 to 1 and lead to the influence of both two types of bifurcations on the trajectories.

3.3 Bifurcations for specific parameters

In order to explain the bifurcations in more detail, now we fix the parameters at

$$\alpha = 9.0, \quad \beta = 14.28, \quad \delta = 0.1 \quad \Omega = 0.01 \tag{16}$$

while the parameters in the piecewise-linear function $f(x)$ are taken as

$$\begin{aligned} &m_0 = -\tfrac{1}{7}, \quad m_1 = \tfrac{2}{7}, \quad m_2 = -\tfrac{3}{7}, \quad m_3 = \tfrac{4}{7}, \\ &Q_1 = 1.0, \quad Q_2 = 2.15, \quad Q_3 = 3.6, Q_4 = +\infty, \end{aligned} \tag{17}$$

which is plotted in Fig. 2. The other related parameters can be computed at $k_1 = \frac{3}{2}$, $k_2 = \frac{31}{12}$, $k_3 = \frac{349}{80}$ because of the continuity of $f(x)$ combining with the condition $k_0 = 0$.

The break points on the piecewise-linear function correspond to six cross sections, denoted by $\Sigma_{\pm i}$: $[(x, y, z) \mid x = \pm Q_i]$, $(i = 1, 2, 3)$, which divide the phase space into seven regions, represented by D_0 and $D_{\pm i}$, $(i = 1, 2, 3)$. In each region, the trajectory is governed by a corresponding linear subsystem, which has a nominal equilibrium orbit, leading to seven **NEO**s, expressed by $\mathbf{NEO}_0$ and $\mathbf{NEO}_{\pm i} (i = 1, 2, 3)$, respectively. Note that the properties of two $\mathbf{NEO}_{\pm i}$ are the same because of the symmetry of the system. The eigenvalues related to $\mathbf{NEO}_0$ and $\mathbf{NEO}_{\pm i} (i = 1, 2, 3)$ can be computed, respectively, as

$$\begin{aligned} &\lambda_1^{(0)} = -9.531, \quad \lambda_{\pm}^{(0)} = -0.0506 \pm 3.596\, I, \\ &\lambda_1^{(\pm 1)} = -13.151, \quad \lambda_{\pm}^{(\pm 1)} = -0.1600 \pm 3.676\, I, \\ &\lambda_1^{(\pm 2)} = -7.148, \quad \lambda_{\pm}^{(\pm 2)} = +0.0524 \pm 3.474\, I, \\ &\lambda_1^{(\pm 3)} = -15.622, \quad \lambda_{\pm}^{(\pm 3)} = -0.2104 \pm 3.702\, I, \end{aligned} \tag{18}$$

from which one may find that $\mathbf{NEO}_{\pm 2}$ are of unstable saddle-type, while other **NEO**s are of stable focus-type. Furthermore, at the cross sections $\Sigma_{\pm 2}$ for $x = \pm 2.15$ and $\Sigma_{\pm 3}$ for $x = \pm 3.6$, the characteristic equations can be, respectively, expressed as

$$\begin{aligned} &\lambda^3 + \left(\frac{493}{70} + \frac{45}{7} q_1\right) \lambda^2 + \left(\frac{3963}{350} + \frac{45}{7} q_1\right) \lambda \\ &\quad + \frac{21573}{250} + \frac{459}{5} q_1 = 0, \\ &\lambda^3 + \left(\frac{113}{70} - 9 q_2\right) \lambda^2 + \left(\frac{7113}{350} - 9 q_2\right) \lambda \\ &\quad + \frac{53703}{250} - \frac{3213}{25} q_2 = 0, \end{aligned} \tag{19}$$

where $q_1, q_2 \in [0, 1]$, from which one may find that for $q_1 = -\frac{143}{450} + \frac{14\sqrt{67}}{450} \approx 0.19153$ and $q_2 = \frac{773}{630} - \frac{2\sqrt{67}}{45} \approx 0.86319$, the two characteristic equations in (17) can be written in the same form as

$$\lambda^3 + \left(5 + \frac{2\sqrt{67}}{5}\right) \lambda^2 + \left(\frac{232}{25} + \frac{2\sqrt{67}}{5}\right) \lambda + \frac{1428}{25} + \frac{714\sqrt{67}}{125}. \tag{20}$$

A pair of pure imaginary eigenvalues as well as a negative real eigenvalue can be obtained, approximated at

$$\lambda_1 = -8.274 \ \lambda_{\pm} = 3.5432\, I, \tag{21}$$

implying a non-smooth Hopf bifurcation occurs, which is of supercritical type demonstrated by further computation.

Remarks:

- The $\mathbf{NEO}_0$ and $\mathbf{NEO}_{\pm i}$, $(i = 1, 2, 3)$ can also be regarded as generalized fixed points, located on the cross section $\Sigma_T : [(x, y, z) \mid \tau = \tau_0 + 2j\pi/, (j = 1, 2, \cdots)]$. In the linear subsystems, they may become foci, centers, saddle points, and even degenerate cusp points. The stabilities of them may influence the trajectory of the whole nonlinear piecewise-linear system.
- Since all the subsystems are linear, a fold or a Hopf bifurcation cannot result in the jumping phenomenon or limit cycle related to the generalized fixed point. However, at the break points, such types of non-smooth bifurcations may cause the trajectory to behave in the corresponding characteristics.

4 Evolution of bursting oscillations as well as the mechanism

Because of the order gap between the exciting frequency and the natural frequency, bursting oscillations, which always behave as a combination of small- and large-amplitude oscillations, can be observed. For the parameters fixed in (14) and (15), the evolution of bursting oscillations with the variation in the parameter A will be investigated, since the amplitude of the external excitation may determine whether the trajectory passes across the break points or not. We find that when A is small, for example, $A = 5.0$, only periodic movements with the frequency Ω in (3) are observed, since the trajectory does not pass across any break points. With the increase in A, the amplitude of the periodic oscillation may pass across the break points, which leads to bursting oscillations. Now, we discuss the bursting oscillations in dependence on A. Here, we focus on two typical cases with $A = 20.0$ (Case A) and $A = 40.0$ (Case B), respectively, in which the trajectories of the bursting oscillations may pass across different numbers of non-smooth cross sections.

All the numerical results of the phase portraits as well as the related time histories following are obtained by the four-order variable step Runge–Kutta method, with the step length $\Delta\tau = 0.0001$ and the initial condition $(x_0, y_0, z_0) = (0.1, 0.1, 0.1)$.

4.1 Bursting oscillations for Case A

For the case with $A = 20.0$, only two non-smooth cross sections $\Sigma_{\pm 1}$ for $x = \pm 1.0$ involve the trajectory of the oscillations. The two cross sections divide the phase space into three regions D_0 and $D_{\pm 1}$ corresponding to three different stable nominal equilibrium orbits, denoted by $\mathbf{NEO}_0$ and $\mathbf{NEO}_{\pm 1}$, governed by three linear subsystems, respectively.

Bursting oscillations Figure 3 gives the phase portrait of the bursting oscillations for $A = 20.0$, and the related time history of y is plotted in Fig. 4.

It can be found that the phase portrait keeps the symmetric property of the original system, while the trajectory passes across three regions D_0 and $D_{\pm 1}$, which can be divided into four segments by the two cross sections $\Sigma_{\pm 1}$, determined by the break points with $x = \pm 1$. Abrupt changes can be observed when the trajectory moves at the non-smooth boundaries because of the abrupt changes in the governing linear subsystems.

From the time history in Fig. 4, it can also be found that the variables may alternate at the break points between two types of stages corresponding to almost

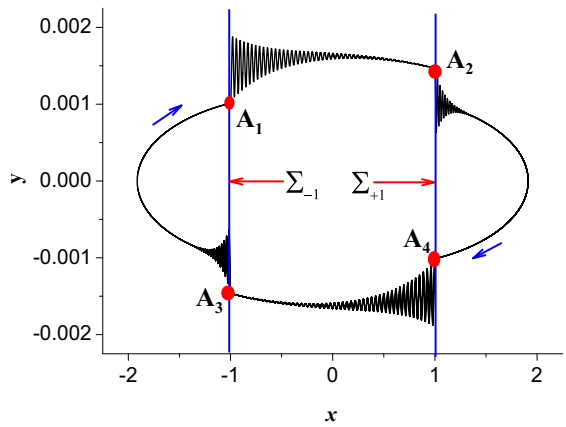

Fig. 3 Phase portrait on the (x, y) plane for $A = 20.0$

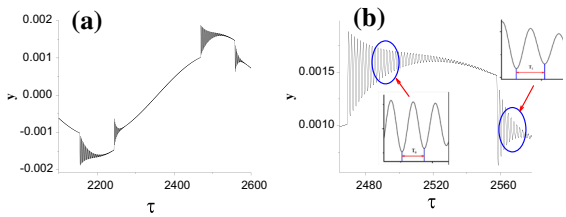

Fig. 4 **a** Time history of y and **b** locally enlarged time history of y for $A = 20.0$

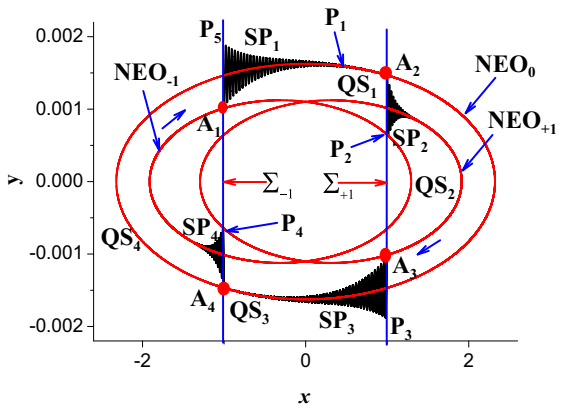

Fig. 5 Overlap of the phase portrait and the **NEO**s

no oscillation and large-amplitude oscillations, respectively, i.e., between quiescent states and repetitively spiking states.

The trajectory of the bursting oscillations in Fig. 3 consists of four stages of quiescent states (**QS**s) and four repetitive spiking states (**SP**s), connected by the breaking points at the switching boundaries.

Mechanism To reveal the mechanism of the bursting oscillations, we plot the overlap of the phase portrait and all the possible **NEO**s of the linear subsystems in Fig. 5. Note that there exist only three **NEO**s since the trajectory only passes across two cross section $\Sigma_{\pm 1}$ with $x = \pm 1$, implying that the phase space of the trajectory can be divided into three regions, in which there exists sole stable **NEO**, respectively.

The trajectory, starting from the point $\mathbf{P}_1$, moves around $\mathbf{NEO}_0$ with small-amplitude oscillations and finally settles down to $\mathbf{NEO}_0$ to form $\mathbf{QS}_1$, since between the two cross sections $\Sigma_{\pm 1}$, the vector field is linear and $\mathbf{NEO}_0$ is a stable attractor. When the trajectory arrives at the point at $\mathbf{A}_2$, located on the switching boundary Σ_{+1}, it may tend to $\mathbf{NEO}_{+1}$, which is a stable attractor for the linear subsystem between the two cross sections Σ_{+1} and $\Sigma_{+2} : [(x, y, z) \mid x = 2.15]$, leading to repetitive spiking oscillations with large-amplitude $\mathbf{SP}_2$, since the trajectory at the point $\mathbf{A}_2$ is not exactly on the focus-type $\mathbf{NEO}_{+1}$.

The repetitive $\mathbf{SP}_2$ settles down to $\mathbf{NEO}_{+1}$ gradually because of the sole stable $\mathbf{NEO}_{+1}$ in the linear subsystem between the two cross sections Σ_{+1} and $\Sigma_{+2} : [(x, y, z)|x = 2.15]$, which leads to the second stage of quiescence ($\mathbf{QS}_2$). The trajectory then moves almost strictly along $\mathbf{NEO}_{+1}$ until it arrives at the point $\mathbf{A}_3$, located on the cross section Σ_{+1} with $x = +1$. When the trajectory passes across the switching boundary Σ_{+1}, it may tend to the sole stable $\mathbf{NEO}_0$ between the two cross sections $\Sigma_{\pm 1}$, in which the vector field is governed by another linear subsystem. Repetitive spiking $\mathbf{SP}_3$ occurs since there exist some distance between the point $\mathbf{A}_3$ and focus-type $\mathbf{NEO}_0$.

The amplitudes of the oscillations of $\mathbf{SP}_3$ decrease gradually, and the trajectory finally settles down to $\mathbf{NEO}_0$ to form $\mathbf{QS}_3$. When the trajectory moves at the point $\mathbf{A}_4$, located on the cross section Σ_{-1}, repetitive spiking $\mathbf{SP}_4$ occurs for the similar reason. The spiking oscillations will settle down to $\mathbf{NEO}_{-1}$ to form $\mathbf{QS}_4$ until the trajectory arrives at the point $\mathbf{A}_1$, located on Σ_{-1}. Repetitive spiking $\mathbf{SP}_1$ takes place, which may finally settle down to $\mathbf{NEO}_0$ to form the quiescence $\mathbf{QS}_1$. Once the trajectory arrives at the starting point $\mathbf{P}_1$, one period of the movement is finished.

Oscillations in **SP***s* The frequency as well as amplitudes of the oscillations of the repetitive spiking $\mathbf{SP}_2$ can be approximated by the eigenvalues related to $\mathbf{NEO}_{+1}$. Note that the pair of the complex conjugate eigenvalues of $\mathbf{NEO}_{+1}$ can be expressed as $\lambda_{\pm}^{(2)} = -0.1600 \pm 3.676\,I$, which determines the decrease in the amplitudes as well as the frequency of the oscillations down to $\mathbf{NEO}_{+1}$. The frequency can be computed at $\Omega_2 = 3.676$, which agrees well with the numerical simulation in Fig. 4 at $\Omega_{2N} = \frac{2\pi}{T_0} = \frac{2\pi}{1.722} = 3.645$.

The decrease in the amplitudes of the oscillation in the y-direction may be approximately described by $Y_{A2}e^{-0.160\tau}$, where Y_{A2} is the y-distance from the point $\mathbf{A}_2$ to $\mathbf{NEO}_{+1}$, i.e., the y-distance between $\mathbf{NEO}_0$ and $\mathbf{NEO}_{+1}$ at $x = 1$, approximated at $Y_{A2} \approx 0.00045$. Therefore, one may approximate the y-distance between the point $\mathbf{P}_2$ and $\mathbf{NEO}_{+1}$ at $Y_{P2} = Y_{A2}e^{-0.160\times 3.645/2} = 0.00036$, which agrees with the numerical simulation in Fig. 4 at $Y_{P2} = 0.000382$.

Similarly, the frequency as well as the amplitudes of the bursting oscillations $\mathbf{SP}_3$ in Fig. 5 can be approximated by the eigenvalues related to $\mathbf{NEO}_0$. For example, the theoretical frequency can be obtained by the imaginary part of the corresponding complex conjugate eigenvalues at $\Omega_2 = 3.596$, which agrees well with the numerical result in Fig. 4 at $\Omega_{2N} = \frac{2\pi}{T_1} = \frac{2\pi}{1.7292} = 3.6336$.

Remarks:

- For smooth systems with two timescales, regular bifurcations exist at the transitions between **QS**s

and **SP**s. However, for the non-smooth system, the change between **QS**s and **SP**s may be caused by the alternations between different governing subsystems with different attractors at the non-smooth boundaries.

- All the repetitive spiking oscillations in Fig. 5 correspond to the transient process from the points on the cross sections to the stable **NEO**s in different regions, which therefore can be obtained theoretically based on the associated linear subsystems as well as the initial point on the cross sections.

4.2 Bursting oscillations for Case B

With the increase in A, more non-smooth cross sections involve the phase portraits of the dynamical system. For the case with $A = 40$, the trajectory passes across all the six non-smooth boundaries, determined by the break points in Fig. 2, implying that the oscillations visit all the seven regions, divided by the cross sections. Therefore, the trajectory of the system is governed by the seven linear subsystems in turn, which have different types of **NEO**s, leading to more complicated bursting oscillations.

Bursting oscillations Figure 6a gives the phase portrait of the bursting oscillations on the (x, y) plane for $A = 40$, from which one may find that the trajectory passes across the boundaries $\Sigma_{\pm i}$, i $= 1, 2, 3)$ at $x = \pm 1, \pm 2.15, \pm 3.6$, respectively.

To show more details of the trajectory, locally enlarged phase portraits in every neighborhood of the boundaries are presented in Fig. 6b–g, where the trajectory are connected by certain notations, such as $\mathbf{B}_3 \longrightarrow \mathbf{B}_3 \ldots$. Qualitatively changes on the trajectory can be observed at the cross sections, which lead to alternations between quiescent states (**QS**s) and repetitive spiking states (**SP**s). For the periodic bursting oscillation in Fig. 6a, there exist eight types of **QS**s and the same number of **SP**s.

For the trajectory, starting from point $\mathbf{B}_1$, it moves along $\mathbf{B}_1\mathbf{B}_2$ to form $\mathbf{QS}_1$, while at point $\mathbf{B}_2$ on Σ_{-3}, repetitive spiking oscillations $\mathbf{SP}_1$ occurs until the trajectory arrives at the Σ_{-2}. With the evolution of non-dimensional time, the amplitudes of the repetitive spiking decrease gradually to zero along $\mathbf{B}_5\mathbf{B}_6$ to form $\mathbf{QS}_2$. At the point $\mathbf{B}_6$ on the cross section Σ_{-1}, $(\mathbf{SP}_2)$ occurs, resulting in repetitive spiking oscillations, which may settle down to $\mathbf{QS}_3$ along $\mathbf{B}_6\mathbf{B}_7$. At point $\mathbf{B}_8$ on Σ_{+1}, $\mathbf{SP}_3$ takes place, leading to the oscillations around $\mathbf{B}_9\mathbf{B}_9$. When the trajectory passes across the boundary Σ_{+2}, $\mathbf{SP}_4$ occurs, yielding the oscillations between $\mathbf{B}_{10}$ to $\mathbf{B}_{12}$. The boundary Σ_{+2} may cause a decrease in the amplitudes of the oscillations, which finally leads to $\mathbf{QS}_4$ to the point $\mathbf{C}_{11}$ via $\mathbf{C}_{12}$.

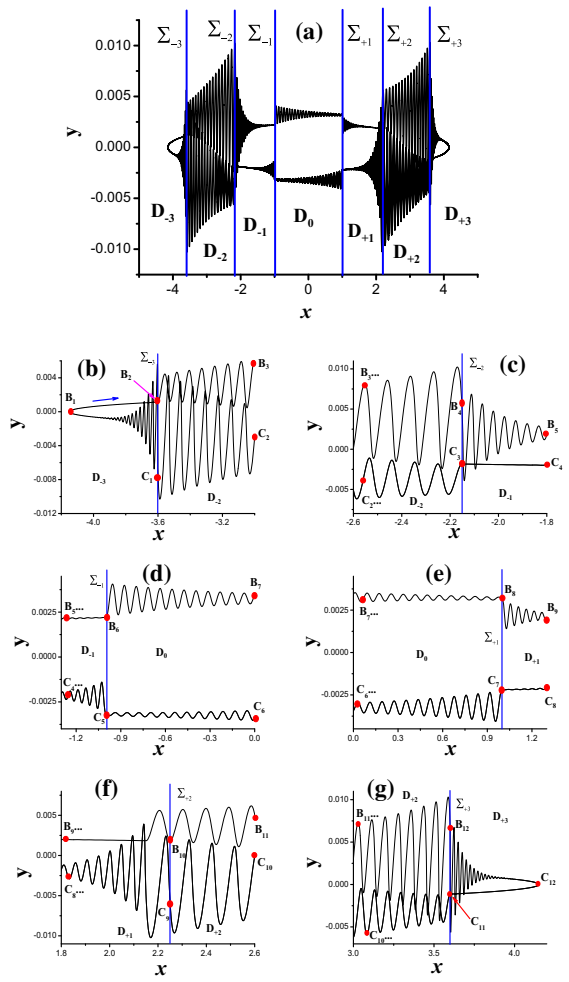

Fig. 6 Phase portrait on the (x, y) plane for $A = 40.0$ and locally enlarged portrait in the neighborhood of $\Sigma_i (i = \pm 1, \pm 2, \pm 3)$ from **b** to **g**

The related time history of y is presented in Fig. 7, which keeps the O_2 symmetry (see the parts $\mathbf{RE}_1$ and $\mathbf{RE}_2$ in Fig. 7a). Therefore, we only need to consider the property of the segment $\mathbf{RE}_1$, which can be extended to another part of the time history. The part $\mathbf{RE}_1$ of the time history is locally enlarged in Fig. 7b–d, from which we see that there exist four stages corresponding

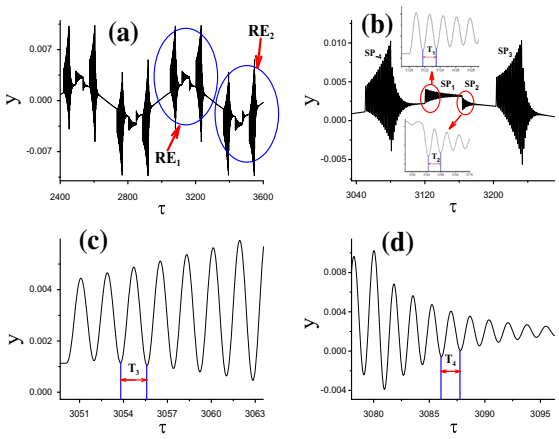

Fig. 7 **a** Time history of y and locally enlarged time history of y in (**b**–**d**)

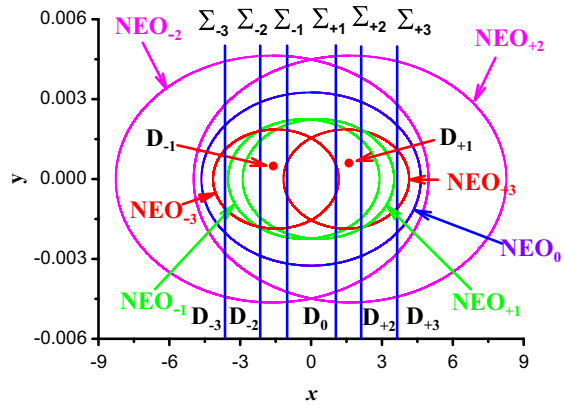

Fig. 8 Non-smooth boundaries and **NEO**s in the different regions

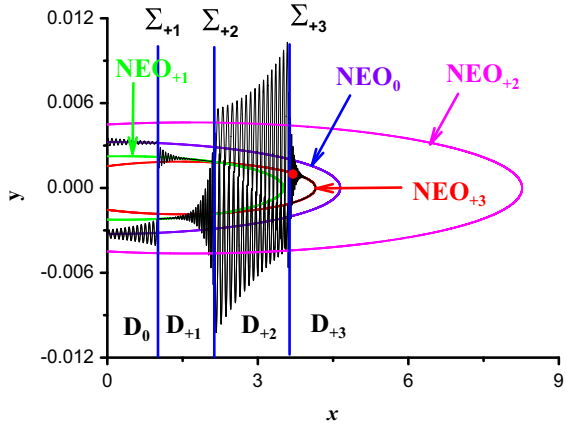

Fig. 9 Overlap of the phase portrait and the **NEO**s for $x \geq 0$

to repetitive spiking $\mathbf{SP}_i$, $(i = 1, 2, 3, 4)$ on the time history.

Now, we turn to the frequencies of different repetitive spiking oscillations via the time history in Fig. 7. We find that the frequencies of $\mathbf{SP}_1$ and $\mathbf{SP}_2$ in Fig. 7b are constants, approximated by $\Omega_{SP1} = \frac{2\pi}{T_1} \approx 3.581$ and $\Omega_{SP2} = \frac{2\pi}{T_2} \approx 3.603$, respectively, which agree very well with the imaginary parts of the pair of complex conjugate eigenvalues related to $\mathbf{NEO}_0$ and $\mathbf{NEO}_{+1}$ in (18) at $\Omega_0 = 3.596$ and $\Omega_{+1} = 3.676$, respectively.

However, the frequencies related to $\mathbf{SP}_{-4}$ and $\mathbf{SP}_3$ in Fig. 7b are not constants. Both the two spiking oscillations can be divided into two parts with different frequency by the non-smooth boundaries. For example, the time history of $\mathbf{SP}_{-4}$ in Fig. 7b is located in Region $\mathbf{D}_{-2}$ and $\mathbf{D}_{-1}$, which can be divided into two parts by the cross section Σ_{-1}, at which the amplitude of the oscillation reaches it maximum value. From the locally enlarged time history in Fig. 7c, d, the frequencies of $\mathbf{SP}_{-4}$ located in $\mathbf{D}_{-2}$ and $\mathbf{D}_{-1}$ can be approximated at $\Omega^{(1)}_{SP1} = \frac{2\pi}{T_3} \approx 3.5392$ and $\Omega^{(1)}_{SP2} = \frac{2\pi}{T_4} \approx 3.681$, respectively.

Mechanism Since there exist six non-smooth boundaries $\Sigma_{\pm i}$, (i = 1, 2, 3), which divide the phase space into seven regions, denoted by $\mathbf{D}_0$ and $\mathbf{D}_{\pm i}$, $(i = 1, 2, 3)$ (see Fig. 8), in each region, there exists one linear subsystem, which results in one **NEO**, respectively. All the seven **NEO**s are presented in Fig. 8, from which one may find that $\mathbf{NEO}_{-i}$ is symmetric to $\mathbf{NEO}_{+i}$, $(i = 1, 2, 3)$, while $\mathbf{NEO}_0$ is symmetric to itself along the axes $x = 0$ and $y = 0$.

Therefore, it is sufficient to only consider the half structure of the phase portrait for $x \geq 0$, which is symmetric to the left half part of the phase portrait. The overlap of the phase portrait and the **NEO**s for $x \geq 0$ is presented in Fig. 9, which can be used to reveal the mechanism of the bursting oscillations.

Figure 10 shows enlarged details of the overlap, from which one reveals that critical changes exist when the trajectory passes across the non-smooth boundaries. Furthermore, the qualitative changes at different break points located on the boundaries are different. For example, at the points $\mathbf{P}_3$ and $\mathbf{Q}_6$ on Σ_{+1}, the trajectory may alternate between small-amplitude oscillations around $\mathbf{NEO}_0$ and small-amplitude oscillations around $\mathbf{NEO}_{+1}$. At the points $\mathbf{P}_6$ on Σ_{+2} and $\mathbf{Q}_2$ on

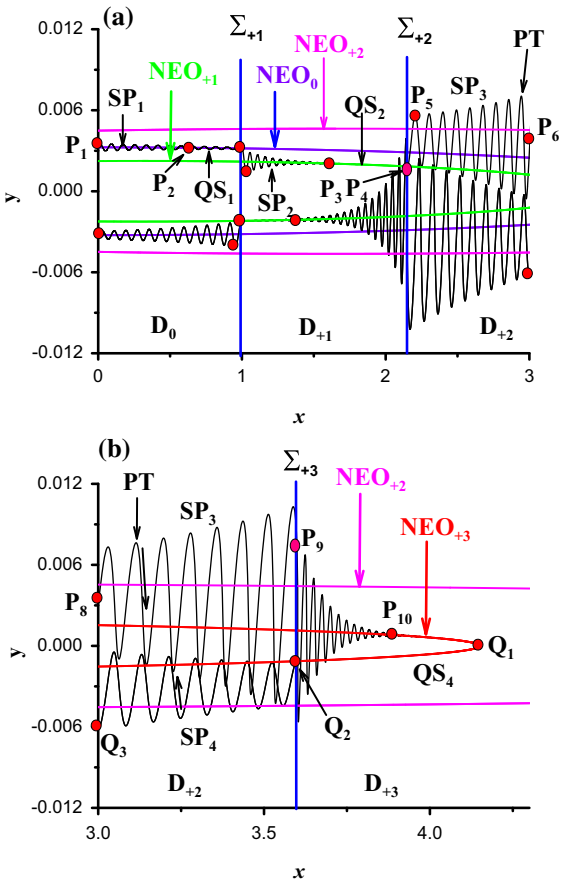

Fig. 10 Locally enlarged overlap **a** for $0 \le x \le 3$ **b** for $x \ge 3$

Σ_{+3}, the trajectory may change from the state which moves almost strictly along a special **NEO** to large-amplitude oscillations, while the points $\mathbf{P}_9$ on Σ_{+3} and $\mathbf{Q}_4$ on Σ_{+2} just separate the large-amplitude oscillations to relatively small-amplitude oscillations.

From above bifurcation analysis, we find that no non-smooth bifurcation occurs at the boundary Σ_{+1}, while at the two boundaries Σ_{+2} and Σ_{+3}, non-smooth super-Hopf bifurcations can be observed. The related frequency can be theoretically computed at $\omega_S = 3.5432$, which agrees very well with the numerical result at $\Omega_{SP1}^{(1)} = \frac{2\pi}{T_3} \approx 3.5392$ via simulation in Fig. 7c. Therefore, the transition of the trajectory between Regions $\mathbf{D}_0$ and $\mathbf{D}_1$ is caused by the non-smooth break points, leading to an attraction of the trajectory to stable $\mathbf{NEO}_0$ and $\mathbf{NEO}_{+1}$, respectively. However, the transitions of the trajectory at the points $\mathbf{P}_6$ on Σ_{+2} and $\mathbf{Q}_2$ on Σ_{+3} between Region $\mathbf{D}_2$ to $\mathbf{D}_3$ or $\mathbf{D}_4$ to $\mathbf{D}_3$ are caused by non-smooth super-Hopf bifurcations, leading to the large-amplitude oscillations with the frequency related to super-Hopf bifurcations.

Now, we turn to the mechanism of the bursting oscillation in Fig. 6. The trajectory, which is locally enlarged in Fig. 10, starting from the point $\mathbf{P}_1$ in Fig. 10a, moves along $\mathbf{NEO}_0$ with oscillations caused by the distance between the starting point and the focus-type stable $\mathbf{NEO}_0$ to form $\mathbf{SP}_1$. The trajectory settles almost down to $\mathbf{NEO}_0$ to form $\mathbf{QS}_1$, at $\mathbf{P}_2$ for example, until it arrives at the break point $\mathbf{P}_3$ at the non-smooth boundary Σ_{+1} for $x = 1$. When the trajectory passes across Σ_{+1}, repetitive spiking ($\mathbf{SP}_2$) occurs, since $\mathbf{P}_3$ is not exactly located on $\mathbf{NEO}_{+1}$, leading to the transient process to the stable $\mathbf{NEO}_{+1}$.

When the trajectory settles down to $\mathbf{NEO}_{+1}$, it moves almost strictly along $\mathbf{NEO}_{+1}$ to form $\mathbf{QS}_2$ until it arrives at the break point $\mathbf{P}_6$ at the non-smooth boundary Σ_{+2} for $x = +2.15$, non-smooth super-Hopf bifurcation takes place, resulting in repetitive spiking oscillations $\mathbf{SP}_3$. The frequency is determined by the frequency associated with the Hopf bifurcation at $\mathbf{P}_6$, though the system is governed by the linear subsystem in Region $\mathbf{D}_{+2}$ with unstable $\mathbf{NEO}_{+2}$. Because of the Hopf bifurcation at $\mathbf{P}_6$, the trajectory does not settle down to stable $\mathbf{NEO}_{+2}$ but oscillates according to the property of the non-smooth Hopf bifurcation.

When the trajectory oscillates via $\mathbf{P}_8$ to $\mathbf{P}_9$, located on the non-smooth boundary Σ_{+3}, a non-smooth Hopf bifurcation occurs, which leads to the disappearance of the oscillations with the frequency related to the Hopf bifurcation. The trajectory then oscillates to settle down to the stable $\mathbf{NEO}_{+3}$, the decrease in the amplitudes of the oscillations can be determined by the real part, while the frequency can be approximated by the imaginary part of the pair of the conjugate eigenvalues related to $\mathbf{NEO}_{+3}$, obtained by the linear subsystem in Region $\mathbf{D}_{+3}$. This is the reason why there exist two frequencies related to $\mathbf{SP}_3$.

When the trajectory settles down to $\mathbf{NEO}_{+3}$ at $\mathbf{P}_{10}$, it moves almost strictly along $\mathbf{NEO}_{+3}$ to form $\mathbf{QS}_4$ until it arrives at the point $\mathbf{Q}_2$, located on Σ_{+2}. A non-smooth Hopf bifurcation occurs, leading to repetitive spiking oscillations $\mathbf{SP}_4$, the frequency of which in Region $\mathbf{D}_{+3}$ can also be estimated by the frequency of non-smooth Hopf bifurcations, though the system is governed by the linear subsystem in Region $\mathbf{D}_{+2}$ with unstable $\mathbf{NEO}_{+2}$.

Once the trajectory oscillates to the point $\mathbf{Q}_4$ at the boundary Σ_{+2}, a non-smooth Hopf bifurcation

causes the transition from oscillations with Hopf bifurcation frequency to oscillations tending to $\mathbf{NEO}_{+1}$. The amplitudes as well as the frequency of $\mathbf{SP}_4$ in Region $\mathbf{D}_{+1}$ can be approximated by the pair of the conjugate eigenvalues related to $\mathbf{NEO}_{+1}$. When the trajectory settles down to $\mathbf{NEO}_{+1}$, it moves almost strictly along $\mathbf{NEO}_{+1}$ to form $\mathbf{QS}_5$ until it arrives at $\mathbf{Q}_6$, located on the non-smooth boundary Σ_{+1}. Transition from $\mathbf{NEO}_{+1}$ to repetitive spiking oscillation $\mathbf{SP}_5$ around $\mathbf{NEO}_0$ is observed, the amplitudes of the oscillations as well as the frequency can be approximated by the pair of complex conjugate eigenvalues related to $\mathbf{NEO}_0$ since the system is governed by the linear subsystem in Region $\mathbf{D}_0$.

The details of the trajectory of the right half side with $x \leq 0$ are symmetric and similar to the above description, which we omit here for simplicity. When the trajectory returns to $\mathbf{P}_1$, one periodic movement of the trajectory is finished, which undergoes eight stages of **QS** and **SP**, respectively. The transition between **QS**s and **SP**s may be caused by the break points to jump between different **NEO**s in associated regions or caused via non-smooth Hopf bifurcations to alternate between **NEO**s and repetitive spiking with large-amplitude oscillations.

Remarks:

- When the trajectories pass across more non-smooth cross sections, more linear subsystems involve the phase portraits, which may lead to more complicated behaviors of the bursting oscillations.
- The transitions between **QS**s and **SP**s may be caused by abrupt changes in different subsystems or by non-smooth bifurcations at the non-smooth boundaries.
- The overlap between **NEO**s in different subsystems and the transformed phase portraits which describe the relations between the state variables and the slow-varying exciting term reveal clearly the evolutions of bursting oscillations.

The abrupt changes for the forms of the bursting oscillations with the variation in the parameter A can also be demonstrated by the evolution of Lyapunov exponents, one of which is also zero, while the other three are shown in Fig. 11.

From Fig. 11, it can be found that all the three Lyapunov exponents are negative with the variation in A, which implies that no chaos phenomenon can be found in the oscillator. However, the largest Lyapunov exponent may reach its extreme values when $A = 8.6293$, $A = 22.9524$, and $A = 31.6229$, respectively, which corresponds to the situations that the extreme values of x of the trajectories just reach the break points of the piecewise-linear function at $x = 1.0, x = 2.15$ and $x = 3.6$, respectively. Therefore, the values of exciting amplitude A when the largest Lyapunov exponent

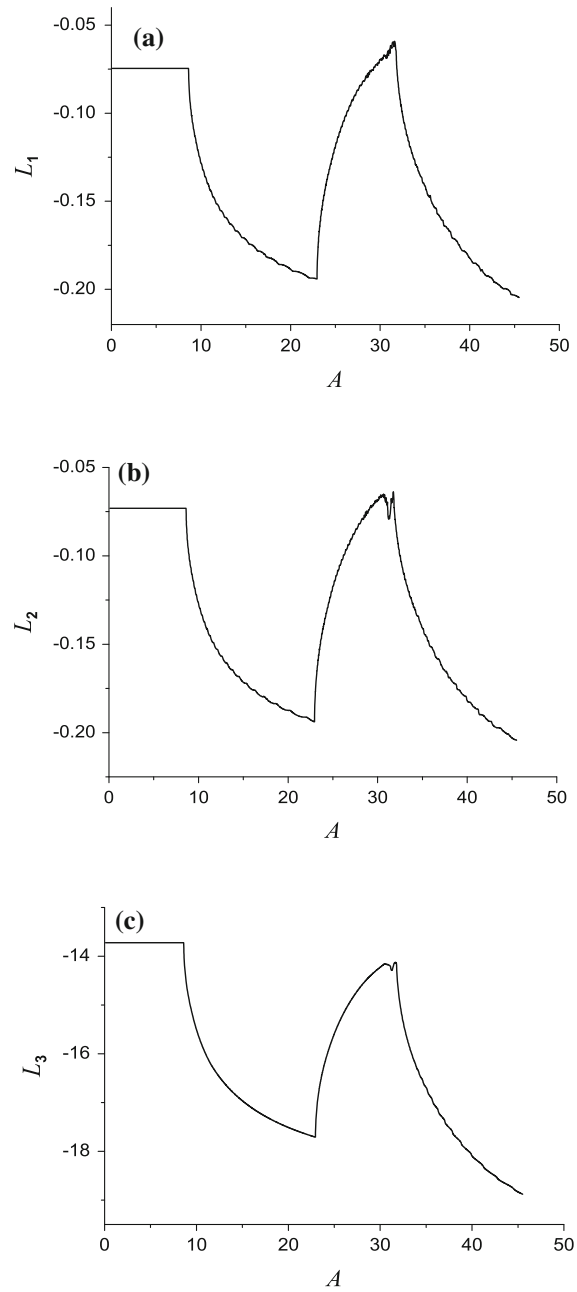

Fig. 11 Three Lyapunov exponents with the variation in A

reaches its extreme values correspond to the separations of different forms of oscillations of the system.

5 Conclusions

Bursting oscillations have been observed in periodically excited piecewise-linear dynamical system with an order gap between the exciting frequency and the natural frequency. For the case when the exciting frequency is far less than the natural frequency, the whole exciting term $w = A\sin(\Omega t)$ can be regard as a slow-varying parameter and used as a bifurcation parameter. The corresponding bifurcations with the variation in w can be employed to account for the critical changes in the trajectories via the transformed phase portraits, which describe the relationships between the state variables and w.

Furthermore, when multiple segments exist in the continuous piecewise-linear functions, multiple cross sections determined by the break points divided the phase space into several regions corresponding to different linear subsystems, which behave in different **NEO**s. With the increase in the amplitude of the excitation, the trajectory may pass across different numbers of cross sections, leading to different forms of bursting attractor.

Unlike the connections between **QS**s and **SP**s via regular bifurcations in smooth vector fields, for the bursting oscillations in piecewise-linear systems, the transitions between **QS**s and **SP**s may be caused by non-smooth bifurcations or the critical changes caused by the abrupt alternations between two different subsystems on both sides of non-smooth boundaries.

Here, we would like to suggest that the special forms of movements in bursting oscillations should be considered when multiple scales in frequency domain involve the practical non-smooth systems, since such types of movements may exist, which may influence the properties of the systems.

Acknowledgments The authors are supported by the National Natural Science Foundation of China (21276115, 11272135, 11472115, 11472116).

References

1. Kiss, A.M., Marx, B., Mourot, G., Schutz, G., Ragot, J.: State estimation of two-time scale multiple models. Application to wastewater treatment plant. Control Eng. Pract. **19**, 1354–1362 (2011)
2. Kess, M., Brning, C., Engel, V.: Multiple time scale population transfer-dynamics in coupled electronic states. Chem. Phys. **442**, 26–30 (2014)
3. Abobda, L.T., Woafo, P.: Subharmonic and bursting oscillations of a ferromagnetic mass fixed on a spring and subjected to an AC electromagnet. Commun. Nonlinear Sci. Numer. Simul. **17**, 3082–3091 (2012)
4. Courbage, M., Maslennikov, O.V., Nekorkin, V.I.: Synchronization in time-discrete model of two electrically coupled spike-bursting neurons. Chaos Solitons Fractals **45**, 645–659 (2012)
5. Bi, Q.S.: The mechanism of bursting phenomena in BZ chemical reaction with multiple time scales. Sci. China Ser. E **10**, 2820–2830 (2012)
6. Simo, H., Woafo, P.: Bursting oscillations in electromechanical systems. Mech. Res. Commun. **38**, 537–541 (2011)
7. Izhikevich, E.: Neural excitability, spiking and bursting. Int. J. Bifurc. Chaos **10**, 1171–1266 (2000)
8. Gaiko, V.A.: Multiple limit cycle bifurcations of the FitzHugh–Nagumo neuronal model. Nonlinear Anal. Theory Methods Appl. **74**, 7532–7542 (2011)
9. Li, X.H., Bi, Q.S.: Cusp bursting and slow-fast analysis with two slow parameters in photosensitive Belousov–Zhabotinsky reaction. Chin. Phys. Lett. **30**, 070503 (2013)
10. Yang, Z.Q., Lu, Q.S., Gu, H.G., Ren, W.: Integer multiple spiking in the stochastic Chay model and its dynamical generation mechanism. Phys. Lett. A **299**, 499–506 (2002)
11. Rasmussen, A., Wyller, J., Vik, J.O.: Relaxation oscillations in spruce–budworm interactions. Nonlinear Anal. Real World Appl. **12**, 304–319 (2011)
12. Watts, M., Tabak, J., Zimliki, C., Sherman, A., Bertram, R.: Slow variable dominance and phase resetting in phantom bursting. J. Theor. Biol. **276**, 218–228 (2011)
13. Han, A.J., Jiang, B., Bi, Q.S.: Symmetric bursting of focus-focus type in the controlled Lorenz system with two time scales. Phys. Lett. A **373**, 3643–3649 (2009)
14. Bi, Q.S., Zhang, Z.D.: Bursting phenomena as well as the bifurcation mechanism in controlled Lorenz oscillator with two time scales. Phys. Lett. A **375**, 1183–1190 (2011)
15. Han, X.J., Bi, Q.S.: Bursting oscillations in Duffing's equation with slowly changing external forcing. Commun. Nonlinear Sci. Numer. Simul. **16**, 4146–4152 (2011)
16. Yi, G.S., Wang, J., Wei, X.L., Deng, B., Li, H.Y., Han, C.X.: Dynamic analysis of Hodgkins three classes of neurons exposed to extremely low-frequency sinusoidal induced electric field. Appl. Math. Comput. **231**, 100–110 (2014)
17. Grgoire-Lacoste, F., Jacquemet, V., Vinet, A.: Bifurcations, sustained oscillations and torus bursting involving ionic concentrations dynamics in a canine atrial cell model. Math. Biosci. **250**, 10–25 (2014)
18. Medetov, M., Weiß, R.G., Zhanabaev, Z.Z., Zaks, M.A.: Numerically induced bursting in a set of coupled neuronal oscillators. Commun. Nonlinear Sci. Numer. Simul. **20**, 1090–1098 (2015)
19. Goussis, D.A.: The role of slow system dynamics in predicting the degeneracy of slow invariant manifolds: the case of vdP relaxation–oscillations. Phys. D **48**, 16–32 (2013)
20. Bi, Q.S., Zhang, R., Zhang, Z.D.: Bifurcation mechanism of bursting oscillations in parametrically excited dynamical system. Appl. Math. Comput. **243**, 482–491 (2014)

21. Li, X.H., Bi, Q.S.: Forced bursting and transition mechanism in CO oxidation with three time scales. Chin. Phys. B **22**, 040504 (2013)
22. Arts, J.C., Llibre, J., Medrado, J.C., Teixeira, M.A.: Piecewise linear differential systems with two real saddles. Math. Comput. Simul. **95**, 13–22 (2014)
23. Zhang, C., Bi, Q.S., Han, X.J., Zhang, Z.D.: On two-parameter bifurcation analysis of switched system composed of Duffing and van der Pol oscillators. Commun. Nonlinear Sci. Numer. Simul. **19**, 750–757 (2014)
24. Zhang, Z.D., Li, Y.Y., Bi, Q.S.: Routes to bursting in a periodically driven oscillator. Phys. Lett. A **377**, 975–980 (2013)
25. Chen, Z.Y., Zhang, X.F., Bi, Q.S.: Bifurcations and chaos of coupled electrical circuits. Nonlinear Anal. Real World Appl. **9**, 1158–1168 (2008)
26. Mkaouar, H., Boubaker, O.: Chaos synchronization for master slave piecewise linear systems: application to Chuas circuit. Commun. Nonlinear Sci. Numer. Simul. **17**, 1292–1302 (2012)
27. Baptista, M.S., Caldas, I.L.: Type-II intermittency in the driven double scroll circuit. Phys. D **132**, 325–338 (1999)
28. Ontanon-Garcia, L.J., Jimenez-Lopez, E., Campos-Canton, E., Basin, M.: A family of hyperchaotic multi-scroll attractors in R^n. Appl. Math. Comput. **233**, 522–533 (2014)
29. Trejo-Guerra, R., Tlelo-Cuautle, E., Jimenez-Fuentes, J.M., Sanchez-Lopez, C., Munoz-Pacheco, J.M., Espinosa-Flores-Verdad, G., Rocha-Perez, J.M.: Integrated circuit generating 3- and 5-scroll attractors. Commun. Nonlinear Sci. Numer. Simul. **17**, 4328–4335 (2012)
30. Leine, R.I., Campen, D.H.: Bifurcation phenomena in non-smooth dynamical systems. Eur. J. Mech. A Solids **25**, 595–616 (2006)